

# Dynamical ergodicity DDA reveals causal structure in time series

Cite as: Chaos 31, 103108 (2021); doi: 10.1063/5.0063724

Submitted: 16 July 2021 · Accepted: 10 September 2021 ·

Published Online: 5 October 2021



View Online



Export Citation



CrossMark

Claudia Lainscsek,<sup>1,2,a</sup>  Sydney S. Cash,<sup>3</sup> Terrence J. Sejnowski,<sup>1,2,4</sup> and Jürgen Kurths<sup>5,6,7</sup> 

## AFFILIATIONS

<sup>1</sup>Computational Neurobiology Laboratory, The Salk Institute for Biological Studies, 10010 North Torrey Pines Road, La Jolla, California 92037, USA

<sup>2</sup>Institute for Neural Computation, University of California San Diego, La Jolla, California 92093, USA

<sup>3</sup>Department of Neurology, Massachusetts General Hospital and Harvard Medical School, Boston, Massachusetts 02114, USA

<sup>4</sup>Division of Biological Sciences, University of California San Diego, La Jolla, California 92093, USA

<sup>5</sup>Potsdam Institute for Climate Impact Research (PIK), Potsdam 14473, Germany

<sup>6</sup>Department of Physics, Humboldt University, Berlin 12489, Germany

<sup>7</sup>Centre for Analysis of Complex Systems, World-Class Research Center “Digital Biodesign and Personalized Healthcare”, Sechenov First Moscow State Medical University, Moscow 119991, Russia

**Note:** This paper is part of the Focus Issue, In Memory of Vadim S. Anishchenko: Statistical Physics and Nonlinear Dynamics of Complex Systems.

<sup>a</sup>**Author to whom correspondence should be addressed:** [claudia@salk.edu](mailto:claudia@salk.edu)

## ABSTRACT

Determining synchronization, causality, and dynamical similarity in highly complex nonlinear systems like brains is challenging. Although distinct, these measures are related by the unknown deterministic structure of the underlying dynamical system. For two systems that are not independent on each other, either because they result from a common process or they are already synchronized, causality measures typically fail. Here, we introduce dynamical ergodicity to assess dynamical similarity between time series and then combine this new measure with cross-dynamical delay differential analysis to estimate causal interactions between time series. We first tested this approach on simulated data from coupled Rössler systems where ground truth was known. We then applied it to intracranial electroencephalographic data from patients with epilepsy and found distinct dynamical states that were highly predictive of epileptic seizures.

Published under an exclusive license by AIP Publishing. <https://doi.org/10.1063/5.0063724>

Epilepsy is the fourth most common chronic neurological disorder and affects more than 50 million people worldwide. It is characterized by seizures, periods of unusual behavior, sensations, and, in some cases, loss of awareness. Unpredictable seizures are dangerous and disruptive. Drug resistant seizures require intervention to localize and remove the brain regions where the seizures are initiated. Seizure prediction could allow less invasive intervention but current prediction methods are unreliable. Synchronization and causality are two major aspects of seizures: Causal interactions between cortical areas drive synchrony, and extreme synchrony leads to seizures. Synchronization and causality are related by dynamical similarity. We introduce dynamical ergodicity, a measure of dynamical similarity that is effective under non-stationary conditions that include phase shifts. Dynamical ergodicity is studied first in a chaotic model

system and is then applied to intracranial electroencephalographic (iEEG) recordings from epilepsy patients. We report promising results that may lead to a better understanding of the mechanisms underlying epileptic states and better methods to predict and prevent seizures.

## I. INTRODUCTION

Chaos theory and ergodic theory are both motivated by related questions concerning dynamical systems.<sup>5,10,23</sup> In the classic chaos theory, the dynamics of the system is governed by deterministic dynamical equations without noise or random perturbations. Thus, the statistics of these systems are generated solely by dynamics. In a chaotic system, phase space trajectories at nearby points diverge

exponentially with a positive Lyapunov exponent. Ergodic theory is concerned with whether the trajectory of a dynamical system eventually covers its phase space over time. The Poincaré recurrence theorem<sup>8,9,27,28</sup> states that an ergodic system will, after a sufficiently long but finite time, return to a state arbitrarily close to its initial state. Under certain conditions, the time average of a function along the trajectories of an ergodic system exists almost everywhere and is related to the space average.

Here, the concept of ergodicity is used as the basis for estimating the dynamical similarity of data from multiple sources and is used to improve causality estimates. In applying ergodicity to time series, the temporal average is replaced by a delay differential analysis (DDA) feature for each time series (e.g., EEG recording channels) and the ensemble average is taken over the DDA features from all the time series. If the two are similar, the time series is part of an ergodic or dynamically similar group of time series. This then can be used to estimate the reliability of our causality measure, CD-DDA (cross-dynamical DDA).<sup>16</sup> CD-DDA, along with most causality measures, relies on comparing a model of one time series with a model that includes inputs from another time series. A reduction of the error is interpreted as causal information flow between the two systems that generate the two time series. If two systems are very similar or are already synchronized, they cannot be considered independent and the causality measure might be unreliable.

CD-DDA was introduced in Ref. 16 (and references therein) and put in context to Granger causality (GC),<sup>12</sup> the work of Wiener,<sup>37</sup> alternative and nonlinear Granger causality approaches,<sup>1–3,6,7,13,14</sup> transfer entropy (TE),<sup>4,33</sup> and convergent cross mapping (CCM).<sup>35</sup> More approaches and reviews for causality detection can be found in the study by Smirnov<sup>34</sup> and the focus issue in Chaos.<sup>30,38</sup> In Ref. 16, we introduced CD-DDA and critically compared it to GC, TE, and CCM, and CD-DDA was superior for causality detection.

We first explore how the similarity of systems and synchronization affect causality estimates for unidirectionally coupled Rössler systems where we know the ground truth. The second application is to obtain intracranial electroencephalographic (iEEG) data from an epilepsy patient that was studied previously with DDA.<sup>17</sup> This patient exhibited chimera states in the pre-ictal period before seizures, during which different channels exhibited chaotic and synchronous activity simultaneously. We show that dynamical ergodicity in combination with CD-DDA can detect distinct state changes that are indicative for pre-, post-, and inter-ictal data. Dynamical ergodicity revealed a new pre-pre-ictal state that preceded all seizures. These states lasted from minutes to hours. Since our analysis extended to days of recordings with a high temporal resolution, we were able to find causal connections between brain areas in the pre-pre-ictal states. This is a proof of concept example that distinct dynamical states may exist in some patients. We are currently analyzing over 100 patients with more than 1000 seizures. The results from this analysis will be published in a medical journal.

The paper is organized as follows. Section II introduces dynamical ergodicity and puts it into the context of previously introduced flavors of DDA. Section III applies dynamical ergodicity to unidirectionally coupled Rössler systems and shows how dynamical ergodicity can be used to improve the reliability of causality estimates. In Sec. IV, we then apply the same analysis to iEEG data from a patient with epilepsy and show how dynamical ergodicity

together with causality can identify multiple states that precede all the seizures with high confidence. These results are summarized in Sec. V.

## II. DDA AND DYNAMICAL ERGODICITY

DDA combines differential embeddings with linear and nonlinear nonuniform functional delay embeddings<sup>24,32,36</sup> to relate the current derivatives of a system to the current and past values of the system variables.<sup>15,16,20</sup> Inspired by Planck's "natural units,"<sup>26</sup> the DDA model maps experimental data onto a set of natural embedding coordinates.

For DDA models with two time delays and three terms to reduce complexity, the general nonlinear DDA model is

$$\dot{u}(t) = \sum_{i=1}^3 a_i u(t - \tau_1)^{m_i} u(t - \tau_2)^{n_i} + \rho_u = \mathcal{F}_u + \rho_u, \quad (1)$$

where  $u(t)$  is a time series and  $m_i, n_i, \tau_{1,2} \in \mathbb{N}_0$  and a degree  $m_j + n_j \leq 4$  of nonlinearity. We then use the coefficients  $a_i$  and the least square error  $\rho_u$  between left- and right-hand sides in Eq. (1) as features. Note, that we explicitly added  $\rho_u$  to highlight its use in the dynamical ergodicity DDA measure introduced below. The derivative on the left side is computed using a five-point center derivative algorithm.<sup>21,22</sup> The coefficients  $a_i$  are estimated with numerical singular value decomposition (SVD) to minimize the least square error.<sup>29</sup>

DDA is a two step process. (i) For a new class of data (e.g., epilepsy iEEG data) the best DDA model [i.e., the coefficients  $m_i$  and  $n_i$  in Eq. (1) as well as the delays or fixed parameters  $\tau_{1,2}$ ] that best fits the overall dynamical properties of the system has to be found. This can be done by supervised (maximizing the classification performance) or unsupervised (minimizing the least square error) structure selection from a list of candidate models (see, e.g., Refs. 19 and 20). This step does not have to be repeated for data from the same data class. (ii) As soon as a DDA model is fixed, data can be analyzed by fitting the data to that model and estimating the features or free parameters  $a_i$  in Eq. (1). We usually estimate the parameters from the data without any pre-processing or filtering except normalizing each data window to zero mean and unit variance.

DDA has four flavors (see Fig. 1):

1. Single trial or channel DDA (ST-DDA)<sup>19</sup> is the classical variant developed for analyzing single time series. It can be used for detection and classification problems to assess dynamical differences in data, to find the DDA model that fits the data best, and to assess observability.<sup>11</sup>
2. Cross trial or channel DDA (CT-DDA)<sup>18</sup> determines the overall dynamics of multiple time series simultaneously.
3. Cross-dynamical DDA (CD-DDA)<sup>16</sup> measures causality between two time series.
4. Dynamical ergodicity DDA (DE-DDA) is a combination of ST-DDA and CT-DDA that is used to assess dynamical ergodicity or similarity from data in the following way:

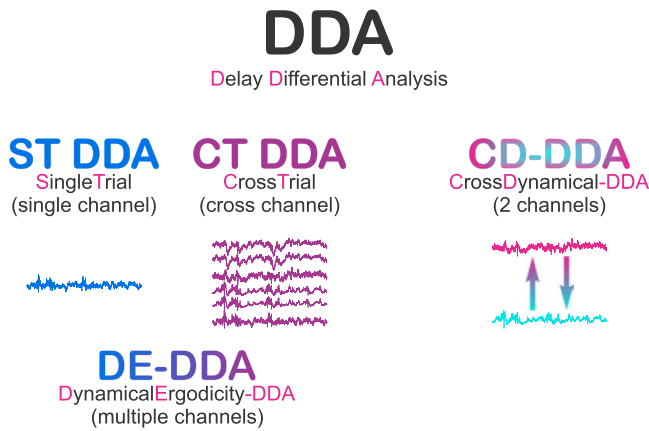


**FIG. 1.** Flavors of DDA: ST-DDA is used for single time series. CT-DDA combines multiple time series to estimate the combined features. DE-DDA combines these two measures to assess dynamical ergodicity. CD-DDA detects causality from two time series.

Consider an ST-DDA model that is applied to a time series  $u(t)$  of length  $L$ ,

$$\begin{aligned} \dot{u}(t) &= a_1 u(t - \tau_1) + a_2 u(t - \tau_2) + a_3 u(t - \tau_1)^2 \\ &= a_1 u_{\tau_1} + a_2 u_{\tau_2} + a_3 u_{\tau_1}^2. \end{aligned} \quad (2)$$

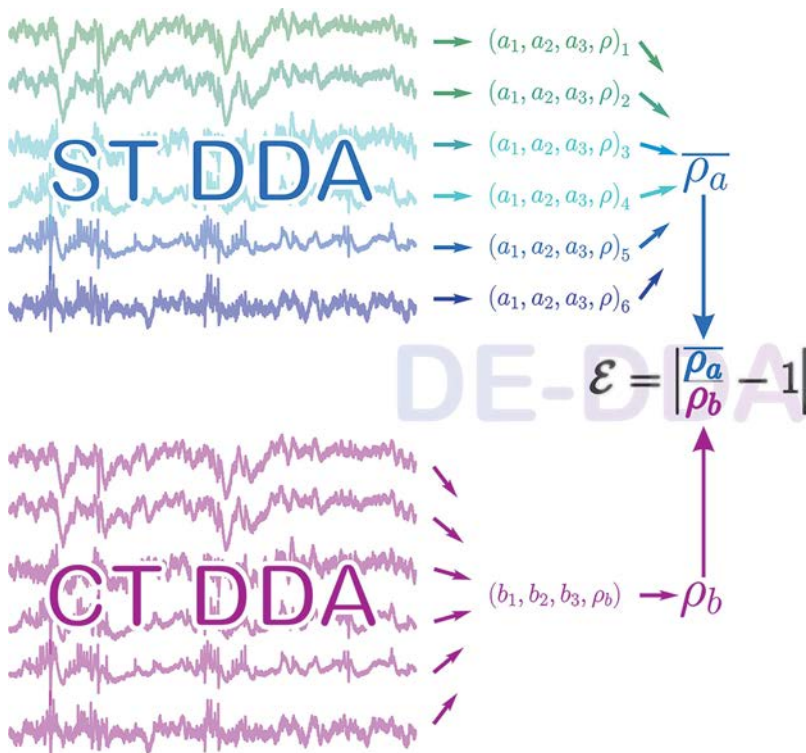


**FIG. 2.** DE-DDA combines ST DDA and CT DDA to test for dynamical ergodicity. An example with six time series is shown, extending the dimensionality in Eq. (6).

The free parameters (features)  $\mathbf{A} = (a_1, a_2, a_3)$  are estimated by solving the equations for  $\mathbf{A}$  using SVD,<sup>29</sup>

$$\begin{pmatrix} \dot{u}(t+1) \\ \dot{u}(t+2) \\ \dot{u}(t+3) \\ \vdots \\ \dot{u}(t+L) \end{pmatrix} = \begin{pmatrix} u(t+1-\tau_1) & u(t+1-\tau_2) & u(t+1-\tau_2)^2 \\ u(t+2-\tau_1) & u(t+2-\tau_2) & u(t+2-\tau_2)^2 \\ u(t+3-\tau_1) & u(t+3-\tau_2) & u(t+3-\tau_2)^2 \\ \vdots & \vdots & \vdots \\ u(t+L-\tau_1) & u(t+L-\tau_2) & u(t+L-\tau_2)^2 \end{pmatrix} \times \begin{pmatrix} a_1 \\ a_2 \\ a_3 \end{pmatrix}, \quad (3)$$

$$\dot{\mathbf{u}} = \mathbf{M}_u \mathbf{A}.$$

Note that  $\mathbf{M}_u$  is an  $(L \times 3)$  matrix. The additional feature is the error,

$$\rho = \sqrt{\frac{1}{L} \sum_{k=1}^L (\mathbf{M}_u \mathbf{A} - \mathbf{B})_k^2}, \quad (4)$$

yielding Eq. (1),

$$\dot{\mathbf{u}} = \mathbf{M}_u \mathbf{A} + \rho_a = \mathcal{F}_u + \rho_u. \quad (5)$$

Note that the error sometimes is denoted by  $\rho_a$  or  $\rho_u$  depending on whether the emphasis is on the time series  $u$  or the features  $\mathbf{A}$ .

Multiple time series can be analyzed with CT-DDA. For two time series,  $u_1(t)$  and  $u_2(t)$ , the features can be either computed for each time series separately, resulting in  $(\mathbf{A}, \rho_a)_1$  and  $(\mathbf{A}, \rho_a)_2$ , or in a

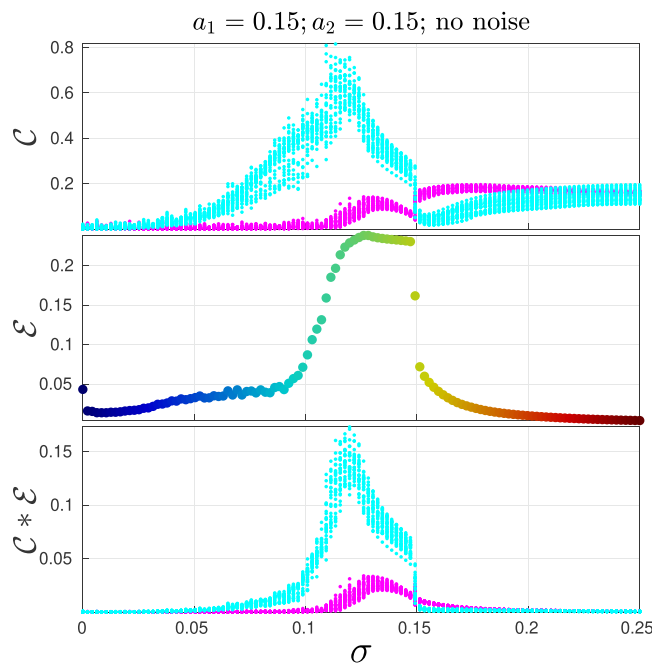
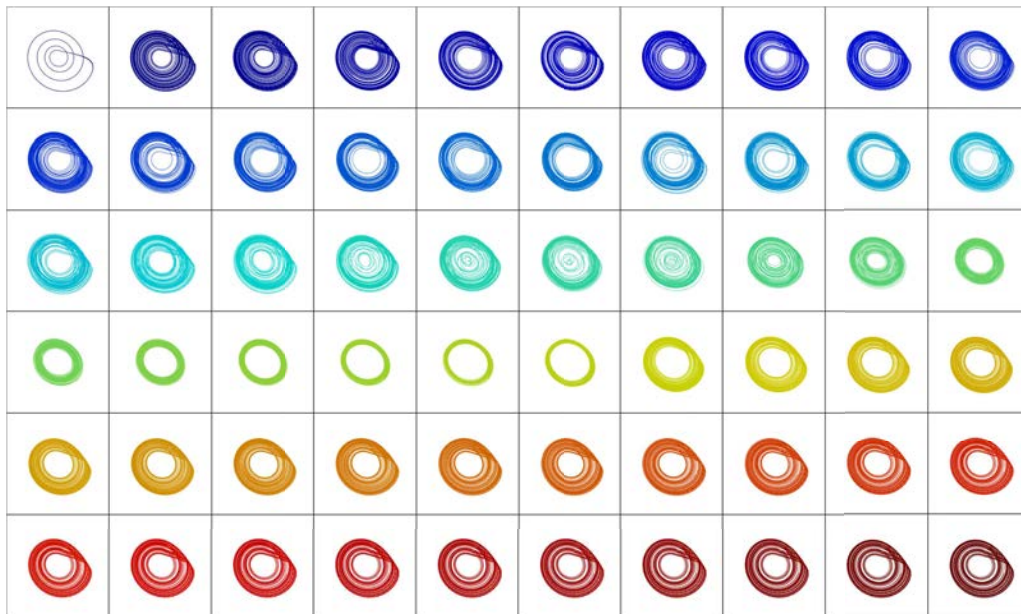


**FIG. 3.** A chaotic Rössler system driving a periodic Rössler system with no noise. In the top plot, the attractors are shown for different coupling strengths. The colors change from blue to red with increasing coupling strength. In the bottom plots,  $\mathcal{C}$  denotes  $C_{uv}$  in cyan and  $C_{vu}$  in magenta.

combined way by solving the equation

$$\begin{pmatrix} \dot{\mathbf{u}}_1 \\ \dot{\mathbf{u}}_2 \end{pmatrix} = \begin{pmatrix} \mathbf{M}_{u_1} \\ \mathbf{M}_{u_2} \end{pmatrix} \mathbf{B}, \tag{6}$$

for the features  $\mathbf{B} = (b_1, b_2, b_3)$ . In (6), the vector  $\begin{pmatrix} \mathbf{B}_1 \\ \mathbf{B}_2 \end{pmatrix}$  has  $2L$  elements since the two time series  $u_1(t)$  and  $u_2(t)$  are each of length  $L$ .  $\begin{pmatrix} \mathbf{M}_{u_1} \\ \mathbf{M}_{u_2} \end{pmatrix}$  is a  $(2L \times 3)$  matrix and  $\mathbf{M}_{u_1}$  and  $\mathbf{M}_{u_2}$  each have the same form as  $\mathbf{M}_u$  in Eq. (3). Therefore,  $\mathbf{B} = (b_1, b_2, b_3)$  is a vector with three elements. This can be extended to any number of time series

(see Fig. 2 for the example of six time series). Note that for ST-DDA, there are as many feature sets  $(\mathbf{A}, \rho_a)$  as there are time series, while for CT-DDA there is only one combined feature vector  $(\mathbf{B}, \rho_b)$ .

CT-DDA only makes sense if the dynamics in the two time series  $u_1(t)$  and  $u_2(t)$  are similar and therefore can be used to test for dynamical similarity. This motivates dynamical ergodicity: Consider two time series  $u_1(t)$  and  $u_2(t)$  and the two corresponding ST-DDA feature vectors  $(\mathbf{A}, \rho_a)_1$  and  $(\mathbf{A}, \rho_a)_2$ . From CT-DDA, there is one combined feature vector  $(\mathbf{B}, \rho_b)$ . The mean of the two ST-DDA errors  $\bar{\rho}_a$  and the CT-DDA error  $\rho_b$  should be similar if the analyzed time series have a similar dynamics and the quotient should be close to one. *Dynamical Ergodicity* as used in DE-DDA is defined as

$$\mathcal{E} = \left| \frac{\bar{\rho}_a}{\rho_b} - 1 \right|. \tag{7}$$

Figure 2 shows an example with six time series. The smaller  $\mathcal{E}$  is, the more similar is the dynamics of the time series under investigation. If both time series are identical,  $\mathcal{E}$  will be zero. Furthermore,  $\mathcal{E}$  is invariant to non-stationarities and phase shifts.

For recordings from patients with epilepsy, it is important to group data from different channels according to their dynamics regardless of phase shifts or non-stationarities in the data. For example, at the onset of a seizure, only data from a few channels might share the same dynamics.

Dynamical ergodicity can be further used to check the reliability of causality. Here, we use CD-DDA as introduced in Ref. 16 to assess causality. For CD-DDA, we consider two dynamical systems  $X$  and  $Y$  resulting in the time series  $u(t)$  and  $v(t)$ . The first step is to compute a set of features  $\mathbf{C} = (c_1, c_2, c_3)$  with

$$\dot{\mathbf{u}} = \mathbf{M}_u \mathbf{C} + \rho_u, \tag{8}$$

where  $\dot{\mathbf{u}}$  is a vector of length  $L$  and the delay matrix  $\mathbf{M}_u$  is a  $(L \times 3)$  matrix. To check if there is a causal connection from  $Y$  to  $X$ , we add the delay matrix from the other time series,  $\mathbf{M}_v$ , to the equation

$$\dot{\mathbf{u}} = (\mathbf{M}_u \mathbf{M}_v) \mathbf{E} + \rho_{uv}. \tag{9}$$

$(\mathbf{M}_u \mathbf{M}_v)$  now is a  $(L \times 6)$  matrix resulting in  $\mathbf{E} = (e_1, e_2, \dots, e_6)$  with six elements. If there is a causal connection from  $Y$  to  $X$ , then the last three elements of  $\mathbf{E}$  will make the model better and the error  $\rho_{uv}$  should decrease. If there is no causal connection from  $Y$  to  $X$ , then the last three elements of  $\mathbf{E}$  will be irrelevant and the error  $\rho_{uv}$  should not change. The difference

$$C_{uv} = |\rho_u - \rho_{uv}| \tag{10}$$

can, therefore, be used to quantify causality from  $Y$  to  $X$ . A causal connection from  $X$  to  $Y$  can be tested in the same way, starting with

$$\dot{\mathbf{v}} = \mathbf{M}_v \mathbf{D} + \rho_v, \tag{11}$$

where  $\dot{\mathbf{v}}$  is a vector of length  $L$  and  $\mathbf{M}_v$  is a  $(L \times 3)$  matrix. Once again, the second delayed matrix  $\mathbf{M}_u$  can be added to the equation,

$$\dot{\mathbf{v}} = (\mathbf{M}_u \mathbf{M}_v) \mathbf{F} + \rho_{vu}. \tag{12}$$

$(\mathbf{M}_u \mathbf{M}_v)$  is the same combined  $(L \times 6)$  delay matrix as in Eq. (9) resulting in  $\mathbf{F}$  with six elements. Whether the first three terms of  $\mathbf{F}$

are relevant or not tells us whether there is a causal connection and

$$C_{vu} = |\rho_v - \rho_{vu}| \tag{13}$$

is used to quantify causality from  $X$  to  $Y$ . However, this and all other causality measures assume that the two dynamical systems are not similar or synchronized to each other. A better causality measure can, therefore, be obtained by multiplying these two measures:  $C * \mathcal{E}$ , where  $C$  is  $C_{uv}$  or  $C_{vu}$ .

### III. UNIDIRECTIONALLY COUPLED RÖSSLER SYSTEMS

Two Rössler systems were unidirectionally coupled by modifying the system in Ref. 25 as explained in Ref. 16,

$$\begin{aligned} \mathbf{R}_1 \begin{cases} \dot{x}_1 = -\omega_1 y_1 - z_1, \\ \dot{y}_1 = x_1 + a_1 y_1, \\ \dot{z}_1 = b - cz_1 + z_1 x_1, \end{cases} \\ \mathbf{R}_2 \begin{cases} \dot{x}_2 = -\omega_2 y_2 - z_2 + \sigma(x_1 - x_2), \\ \dot{y}_2 = x_2 + a_2 y_2, \\ \dot{z}_2 = b - cz_2 + z_2 x_2, \end{cases} \end{aligned} \tag{14}$$

with  $b = 0.2$  and  $c = 10$ . We consider the following two cases: (1) a chaotic Rössler system driving a periodic Rössler system and (2) a periodic Rössler system driving a chaotic Rössler system. In the first case, we set  $\omega_1 = 1.030\ 225$ ,  $\omega_2 = 0.970\ 225$ , and  $a_1 = a_2 = 0.15$ . In the second case, we set  $\omega_1 = 0.970\ 225$ ,  $\omega_2 = 1.030\ 225$ ,  $a_1 = 0.15$ ,

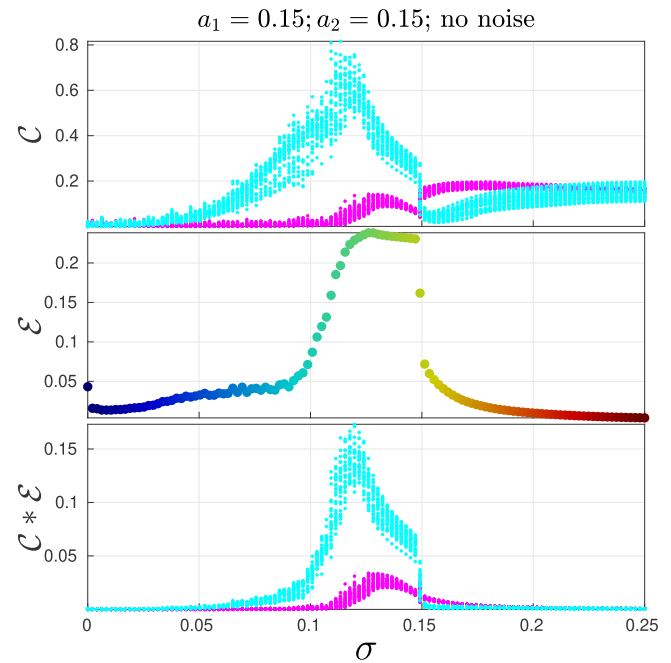
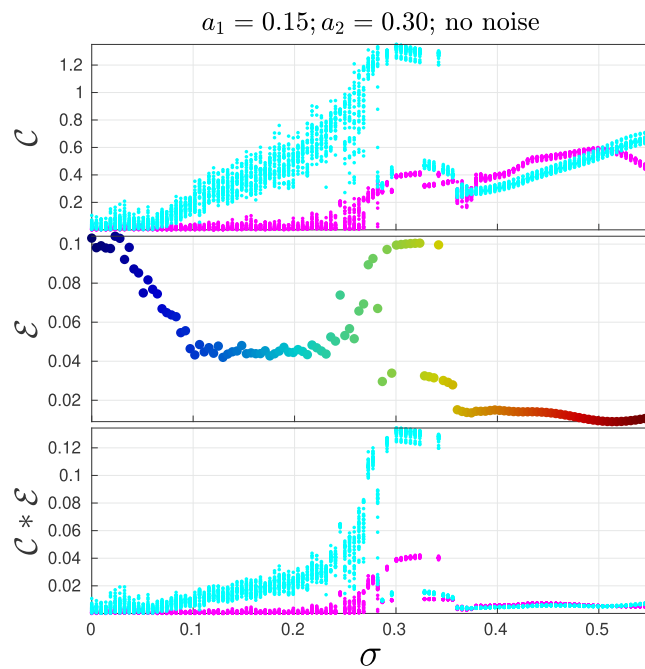
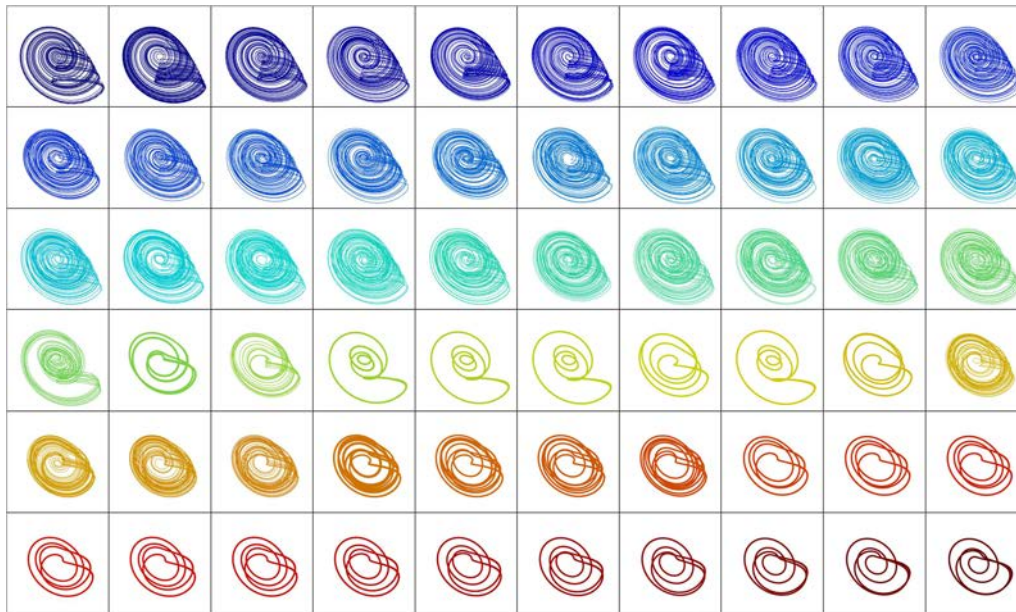


FIG. 4. A chaotic Rössler system driving a periodic Rössler system with high noise. The colors change from blue to red with increasing coupling strength.  $C$  denotes  $C_{uv}$  in cyan and  $C_{vu}$  in magenta. White noise with SNR = 10 dB was added.



**FIG. 5.** A periodic Rössler system driving a chaotic Rössler system with no noise. In the top plot, the attractors are shown for different coupling strengths. The colors change from blue to red with increasing coupling strength.  $C$  denotes here both  $C_{uv}$  (in cyan) and  $C_{vu}$  (in magenta).

and  $a_2 = 0.3$ . The coupling strength  $\sigma$  was varied between 0.001 and 0.25 in the first case and between 0.001 and 0.55 in the second case, each in 120 equally spaced steps. The initial conditions were the same for all numerical experiments. The integration step size  $\delta t$  was set to 0.05 with a transient of 25 000 time points discarded.

DDA was run with a window length of  $6000 \delta t$  and a window shift of  $1554 \delta t$  resulting in 29 windows, the same as in Ref. 16. The same DDA model as in Ref. 16 was used,

$$\mathcal{F}_u = a_1 u_{\tau_1} + a_2 u_{\tau_2} + a_3 u_{\tau_1}^3, \tag{15}$$

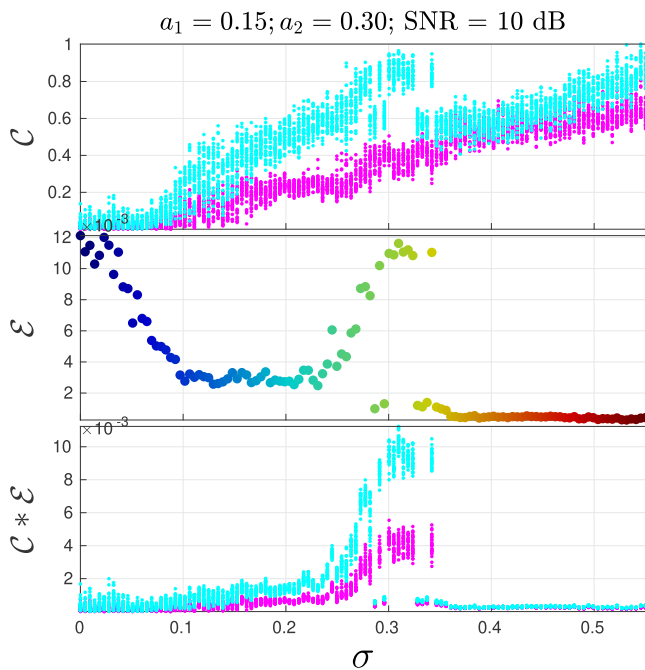


**FIG. 6.** A periodic Rössler system driving a chaotic Rössler system with high noise.  $C$  denotes here both  $C_{uv}$  (in cyan) and  $C_{vu}$  (in magenta). White noise with SNR = 10 dB was added.

with  $u_{\tau_j} = u(t - \tau_j)$ ,  $u = x_{1,2}$ , and the adjusted delays  $\tau_1 = 64 \delta t$  and  $\tau_2 = 18 \delta t$ . The numerical derivatives were estimated with a center derivative as explained in Refs. 21 and 22. We further show the noise-free cases and the case of added white noise to all signals with a signal-to-noise ratio (SNR) of 10 dB.

**A. Chaotic Rössler system driving a periodic Rössler system**

The driven attractors for  $\omega_1 = 1.030\ 225$ ,  $\omega_2 = 0.970\ 225$ , and  $a_1 = a_2 = 0.15$  in Eq. (14) are shown in Fig. 3 with no noise. The colors change in the coupling strength  $\sigma$  from blue to red. The CD-DDA plot, showing  $C$ , for the noise-free case is similar to the one in Ref. 16.  $C$  denotes here both  $C_{uv}$  and  $C_{vu}$  for the corresponding direction of causality. Note the abrupt onset of synchronization at  $\sigma = 0.15$ .

Two problems are apparent in Fig. 3: For small coupling strengths, causality cannot be detected and the direction of causality is reversed when the two systems are synchronized. In the high-noise case, causality cannot be detected for small coupling strengths and is even reversed after synchronization.

The dynamical ergodicity  $\mathcal{E}$  in Eq. (7) is plotted in the middle panels of Figs. 3 and 4.  $\mathcal{E}$  is small when the two time series have similar dynamics. This is the case when the coupling strength is small or when they are synchronized. These are exactly the cases when the causality  $C$  ( $C_{uv}$  and  $C_{vu}$ ) is ambiguous. One possible solution is to use the product  $C * \mathcal{E}$ , as shown in the bottom panels. Without noise, this is very small for the cases where causality makes little sense. For the high-noise case, there is too much noise in the two time series to assess causality because they are similar. Such cases always should be viewed with caution.

**B. Periodic Rössler system driving a chaotic Rössler system**

The driven attractors for  $\omega_2 = 1.030\ 225$ ,  $\omega_1 = 0.970\ 225$ ,  $a_1 = 0.15$ , and  $a_2 = 0.3$  and no noise are shown in Fig. 5. The coupling strength  $\sigma$  was varied between 0.001 and 0.55 in 120 equally spaced steps. In the upper panel, the colors change with the coupling strength  $\sigma$  from blue to red. The driven attractors with noise are shown in Fig. 6 (SNR = 10 dB). In this example, causality  $C$  is detected in the correct direction, except for small coupling strengths

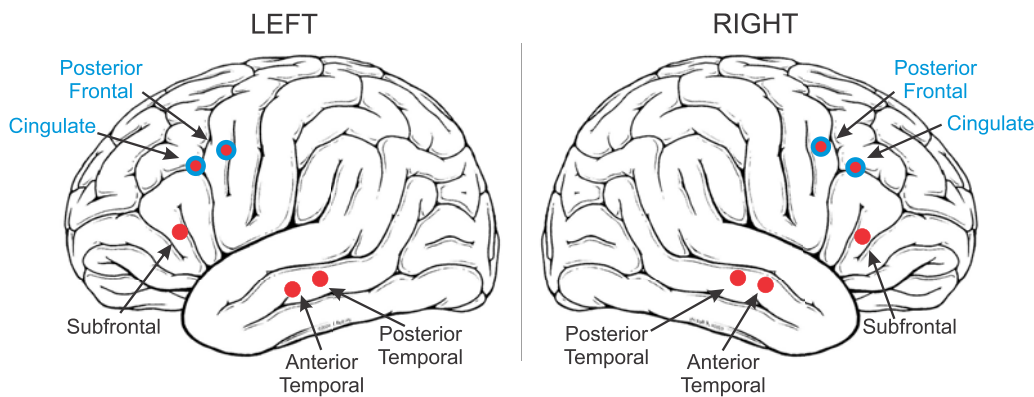


**FIG. 7.** Locations of the implanted iEEG electrodes. The onset channels, as determined by a neurologist, are highlighted in blue. Recordings from the two hemispheres are stacked and displayed in the top and bottom portions of the plots in subsequent figures.

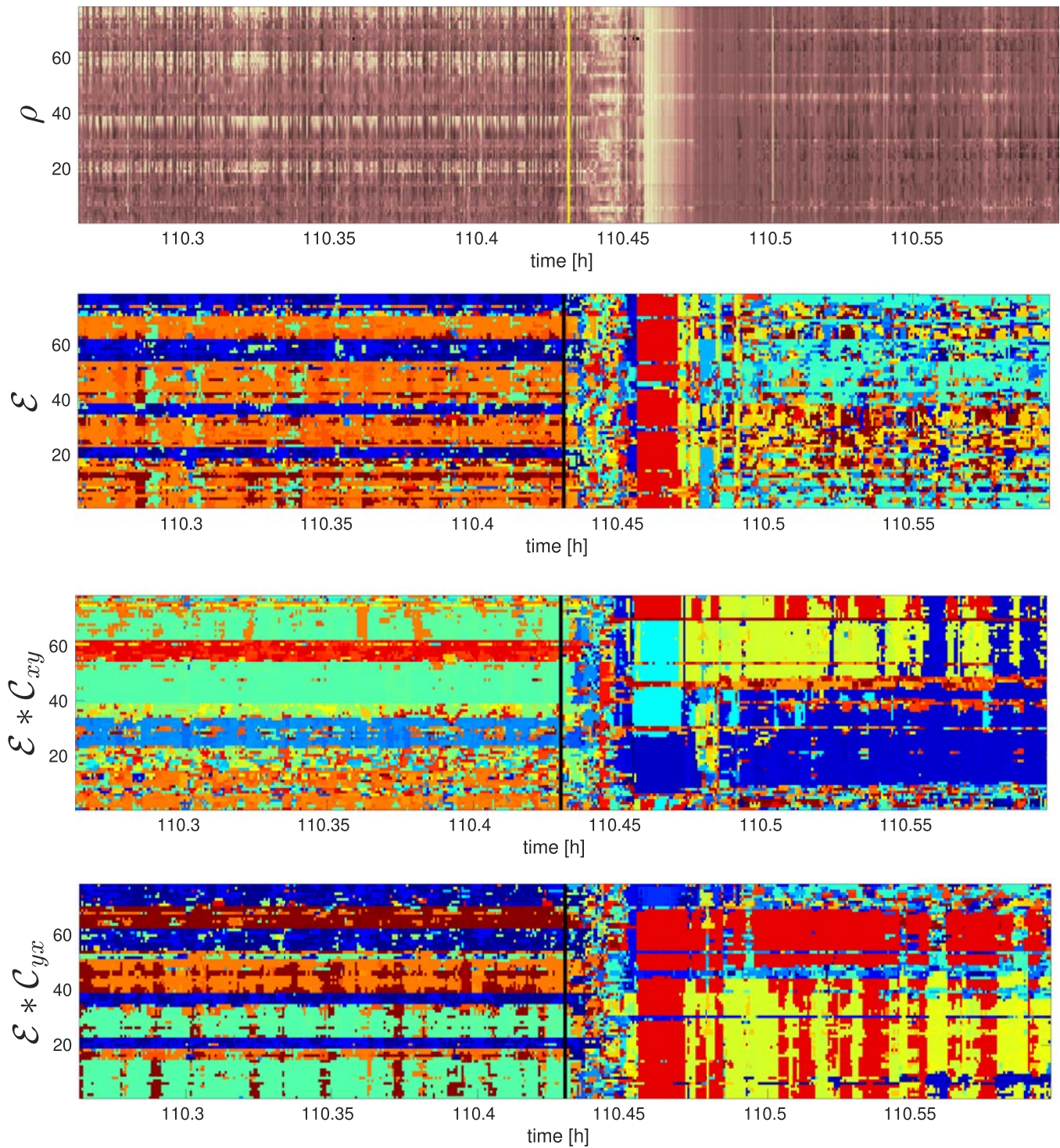


**FIG. 8.** Analysis of 77 channels 10 min before to 10 min after onset of seizure 4. The panels show  $\rho$  and THOSVD analysis of  $\mathcal{E}$ ,  $\mathcal{E} * C_{xy}$ , and  $\mathcal{E} * C_{yx}$ . For  $\rho$  (upper plot), the colors represent the value of  $\rho$ . For the remaining plots, the colors represent communities (see text). The vertical lines near the center indicate the seizure onset as marked by a neurologist. The onset channels are in the red region of the third panel from the top preceding the seizure.

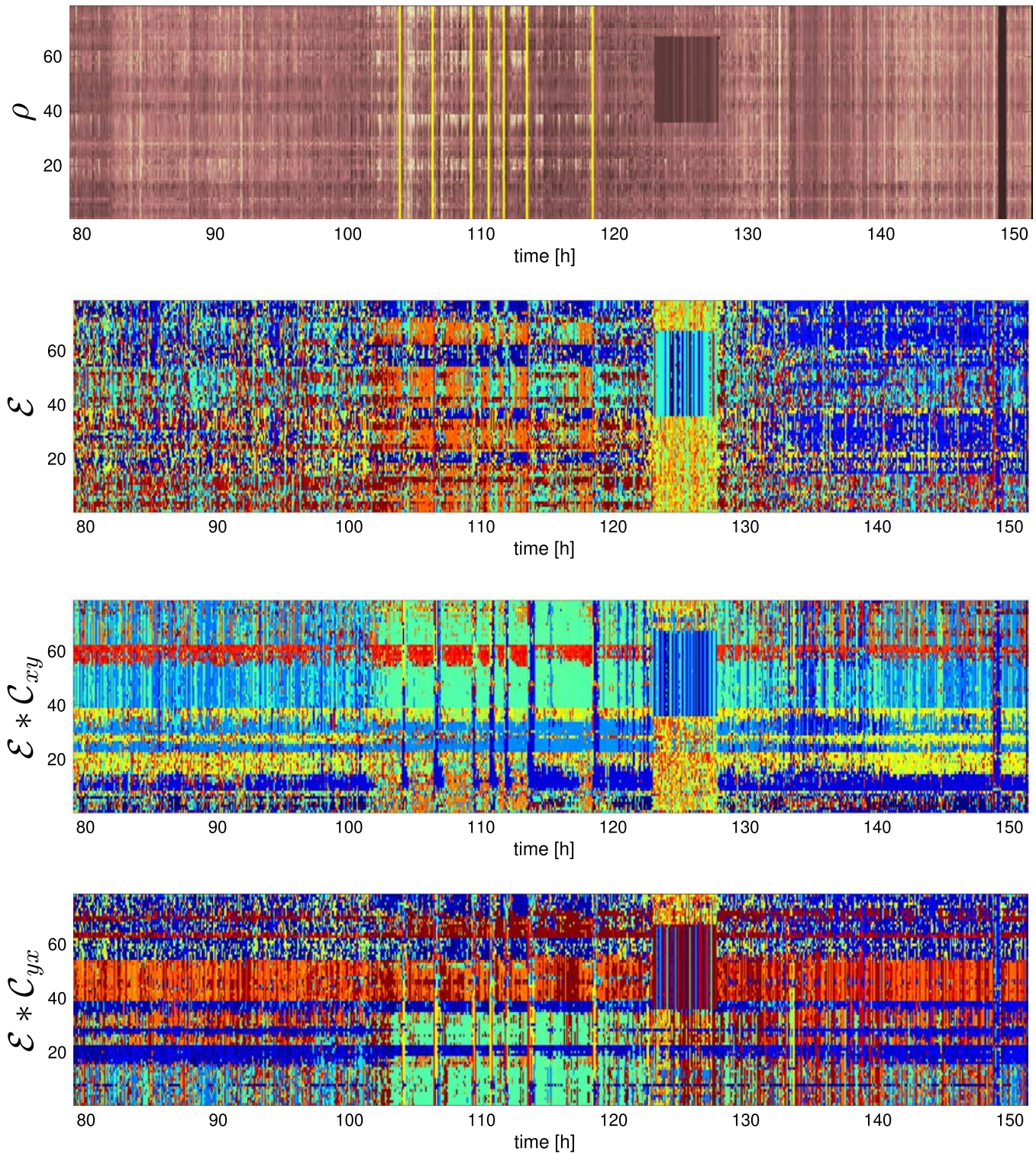


FIG. 9. 72 h of data; 77 channels;  $\rho$  and THOSVD analysis of  $\mathcal{E}$ ,  $\mathcal{E} * C_{xy}$ , and  $\mathcal{E} * C_{yx}$  are shown.

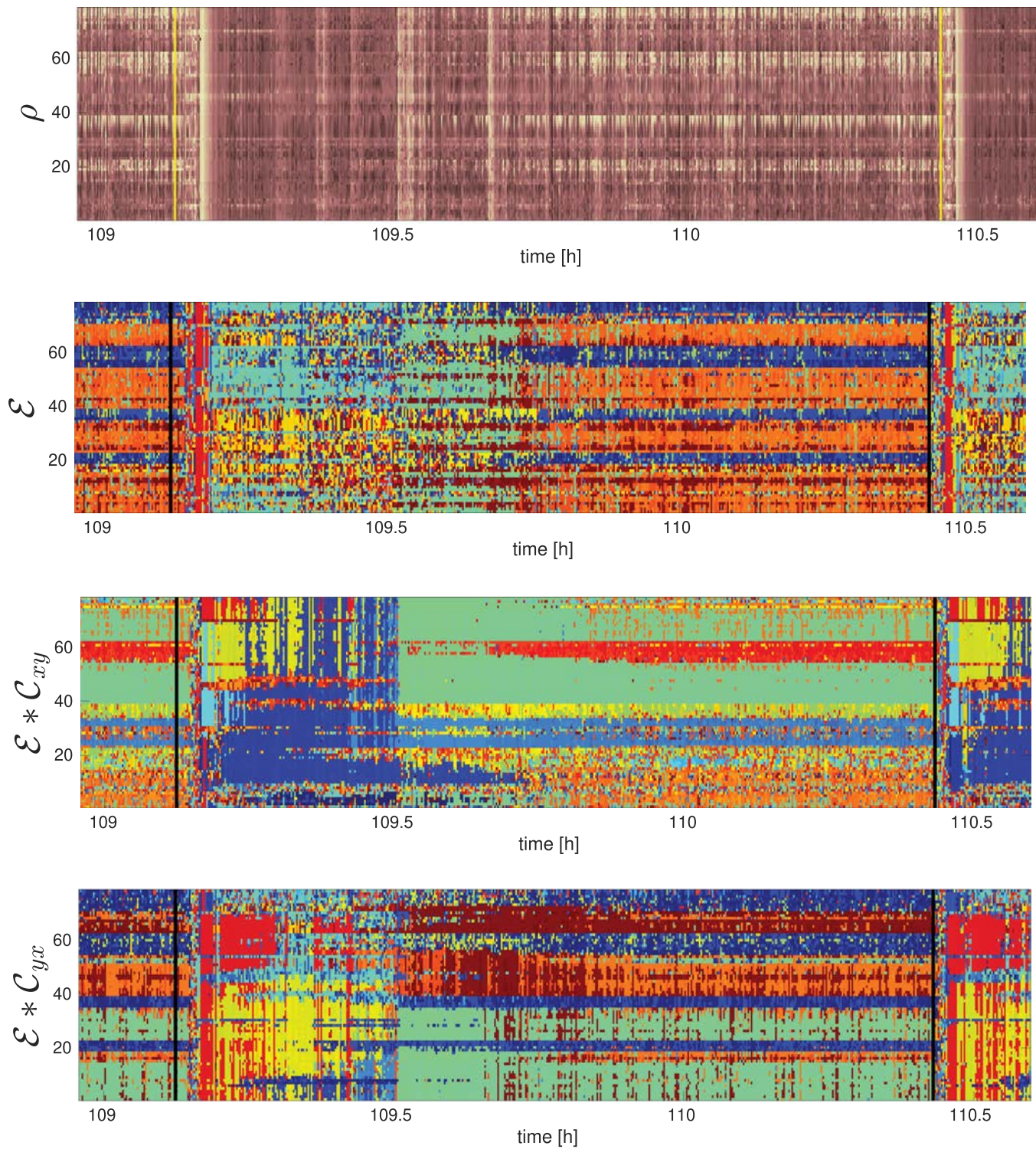


FIG. 10. Seizures 3 and 4.  $\rho$  and THOSVD analysis of  $\mathcal{E}$ ,  $\mathcal{E} * C_{xy}$ , and  $\mathcal{E} * C_{yx}$  are shown.

and after the systems synchronize. Again, dynamical ergodicity  $\mathcal{E}$  helps identify when causality makes sense.

#### IV. CAUSALITY AND DYNAMICAL ERGODICITY IN EPILEPTIC SEIZURES

The causality measures introduced above are applied here to recordings from a patient with epilepsy that were analyzed previously in Ref. 17 using same DDA model,

$$\dot{u} = a_1 u_{\tau_1} + a_2 u_{\tau_2} + a_3 u_{\tau_1}^4 + \rho_u = \mathcal{F}_u + \rho_u, \quad (16)$$

where  $u_{\tau_i} = u(t - \tau_i)$  and  $u(t)$  are iEEG data. The delay pair is  $\tau = (7, 10) \delta t$ , where  $\delta t = \frac{1}{f_s}$  with the sampling rate  $f_s = 500$  Hz. The choice of this model is explained in Refs. 17 and 19. The patient demographics and characteristics are described in Ref. 19. All data analyses were performed under protocols monitored by the Massachusetts General Hospital according to National Institutes of Health guidelines. Figure 7 shows the schematic of the implanted iEEG electrode locations for 77 recording sites.

The ST-DDA features for each channel were computed separately for sliding windows with a length of 250 ms and a window shift of half that length. Additionally, CT-DDA as well as the CD-DDA features were computed for each pair of channels, resulting in 2926 pairwise channel combinations. There were three ( $77 \times 77$ ) matrices ( $\mathcal{E}$ ,  $\mathcal{E} * C_{xy}$ , and  $\mathcal{E} * C_{yx}$ ) for each 250 ms time window. To reduce the dimension by one, truncated higher-order SVD (THOSVD)<sup>19</sup> was performed on 100 time windows (about 13 s) on each of these matrices and then all channels that correlated to the same singular values were identified and given the same color in the figures. Each color, therefore, represents a community.<sup>31</sup>

Figure 8 shows analysis of the recordings 10 min before to 10 min after the onset of seizure 4. The channels were not sorted. A chimera state identified for this patient before this seizure<sup>17</sup> has lighter/whiter colors in the upper plot and belongs to the same community shown in blue in the ergodicity plot, second from the top. The synchronized channels belong to a different community and are shown in orange. The brief green vertical regions are micro events. During the seizure, the kaleidoscope of colors indicate dynamical diversity. After the seizure, most channels become synchronized, as indicated by the vertical red region, which is followed by a shift to another state.

In Fig. 9, a much longer 72-h recording is shown comprising seven seizures, and in Fig. 10, an expansion is shown 10 min before the third seizure to 10 min after the onset of seizure 4. The orange and blue regions are chimera states (explained in detail in Ref. 17) that occur before each of the seven seizures and last for up to 2 h. Importantly, before the chimera states, there are three distinct states of about 10 min each (seen most clearly in Fig. 10). Exactly, the same sequence of states occurs before each seizure and varies only in duration.

This newly identified pre-pre-ictal state before the orange/blue chimera state also appears as a decrease of the blue community around channel 10 in the  $\mathcal{E} * C_{xy}$  plot (third from the top) in Fig. 9 and at 109.5 h in Fig. 10. Red regions increase as blue regions decrease. These blue channels (left posterior temporal, Fig. 7) are outside the seizure onset zone but enable the chimera pre-ictal states. The red channels are the onset channels (right posterior frontal,

Fig. 7). In Fig. 9, the two hemispheres (top half and bottom half) show clear differences in the two lower causality plots but not in the top two plots, reflecting the ability of the causal measure to detect the origin of the seizure in one of the hemispheres.

#### V. DISCUSSION

Dynamical ergodicity  $\mathcal{E}$  was introduced as a measure of dynamical similarity that is invariant to non-stationarities. We then applied  $\mathcal{E}$  to simulated data from two coupled Rössler systems. Channels that are too similar or are synchronized cannot be assessed for causality because these channels are not independent and already share information. By identifying these conditions, dynamical ergodicity can add reliability to any causality measure by focusing analysis on those channels that are more likely to carry causal information. After successfully validating this new causal measure on simulated data, we then applied this analysis on 72 h of iEEG recordings from a patient having seven seizures.

A previously identified pre-ictal chimera state<sup>17</sup> was preceded by a newly identified pre-pre-ictal state that occurs away from the onset channels and has high predictive power for the pre-ictal chimera state. The cortex enters the pre-pre-ictal state early enough for feedback intervention to reduce the severity or possibly prevent the predicted epileptic seizure. These findings from one patient are a proof of concept. Further analysis of recordings from a larger cohort of patients (over 1000 seizures from around 100 patients) will explore the diversity of seizures. A paper is in preparation and will be published in a medical journal.

The ability to detect multiple cortical states and the transitions between them makes it possible to study the dynamic regulation of the cortical activity that occurs during sleep stages and levels of arousal and attention. DDA can be computed in real time and is insensitive to artifacts, opening up the possibility of closing the loop with feedback.

#### ACKNOWLEDGMENTS

C.L. and T.J.S. were supported by the NIH Grant Nos. 5 R01 EB026899-03 and R01 NS104368-03 and also by the Swartz Foundation. J.K. was supported by the Ministry of Science and Higher Education of the Russian Federation within the framework of state support for the creation and development of World-Class Research Centers “Digital biodesign and personalized healthcare” (Grant No. 075-15-2020-926).

#### DATA AVAILABILITY

The data that support the findings of this study are available from the corresponding author upon reasonable request.

#### REFERENCES

- <sup>1</sup>E. Baek and W. Brock, “A general test for nonlinear Granger causality: Bivariate model” (Korea Development Institute, University of Wisconsin-Madison, 1992), Vol. 15, pp. 197–235 (unpublished).
- <sup>2</sup>Z. Bai, Y. Hui, D. Jiang, Z. Lv, W.-K. Wong, and S. Zheng, “A new test of multivariate nonlinear causality,” *PLoS ONE* **13**(1), 1–14 (2018).
- <sup>3</sup>Z. Bai, W.-K. Wong, and B. Zhang, “Multivariate linear and nonlinear causality tests,” *Math. Comput. Simul.* **81**(1), 5–17 (2010).

- <sup>4</sup>L. Barnett, A. B. Barrett, and A. K. Seth, "Granger causality and transfer entropy are equivalent for Gaussian variables," *Phys. Rev. Lett.* **103**, 238701 (2009).
- <sup>5</sup>L. Boltzmann, "Ergoden in chapter III, §32," in *Vorlesungen über Gastheorie*, edited by J. A. B. Leipzig (1898).
- <sup>6</sup>W. Brock, W. Dechert, and J. Scheinkman, "A test for independence based on the correlation dimension" (Department of Economics, 1987) (unpublished).
- <sup>7</sup>W. Brock, W. Dechert, and J. Scheinkman, "A test for independence based on the correlation dimension," *Econometric Rev.* **15**, 197–235 (1996).
- <sup>8</sup>C. Carathéodory, *Über den Wiederkehrrsatz von Poincaré* (Sitzungsberichte, Berlin, 1919), pp. 580–584.
- <sup>9</sup>C. Carathéodory, *Gesammelte Mathematische Schriften V* (C. H. Beck'sche Verlagsbuchhandlung, 1957).
- <sup>10</sup>J. P. Eckmann and D. Ruelle, "Ergodic theory of chaos and strange attractors," *Rev. Mod. Phys.* **57**, 617 (1985).
- <sup>11</sup>C. E. Gonzalez, C. Lainscsek, T. J. Sejnowski, and C. Letellier, "Assessing observability of chaotic systems using delay differential analysis," *Chaos* **30**(10), 103113 (2020).
- <sup>12</sup>C. W. Granger, "Investigating causal relations by econometric models and cross-spectral methods," *Econometrica* **37**, 424–438 (1969).
- <sup>13</sup>P. Grassberger and I. Procaccia, "Measuring the strangeness of strange attractors," *Physica D* **9**, 189 (1983).
- <sup>14</sup>C. Hiemstra and J. D. Jones, "Testing for linear and nonlinear Granger causality in the stock price-volume relation," *J. Finance* **49**(5), 1639–1664 (1994).
- <sup>15</sup>M. Kremliovskiy and J. Kadtke, "Using delay differential equations as dynamical classifiers," *AIP Conf. Proc.* **411**, 57 (1997).
- <sup>16</sup>C. Lainscsek, C. E. Gonzalez, A. L. Sampson, S. S. Cash, and T. J. Sejnowski, "Causality detection in cortical seizure dynamics using cross-dynamical delay differential analysis," *Chaos* **29**(10), 101103 (2019).
- <sup>17</sup>C. Lainscsek, N. Rungratsameetaweemana, S. S. Cash, and T. J. Sejnowski, "Cortical chimera states predict epileptic seizures," *Chaos* **29**(12), 121106 (2019).
- <sup>18</sup>C. Lainscsek, A. L. Sampson, R. Kim, M. L. Thomas, K. Man, X. Lainscsek, The COGS Investigators, N. R. Swerdlow, D. L. Braff, T. J. Sejnowski, and G. A. Light, "Nonlinear dynamics underlying sensory processing dysfunction in schizophrenia," *Proc. Natl. Acad. Sci. U.S.A.* **116**(9), 3847–3852 (2019c).
- <sup>19</sup>C. Lainscsek, J. Weyhenmeyer, S. S. Cash, and T. J. Sejnowski, "Delay differential analysis of seizures in multichannel electrocorticography data," *Neural Comput.* **29**(12), 3181–3218 (2017).
- <sup>20</sup>C. Lainscsek, J. Weyhenmeyer, M. Hernandez, H. Poizner, and T. Sejnowski, "Non-linear dynamical classification of short time series of the Rössler system in high noise regimes," *Front. Neurol.* **4**, 182 (2013).
- <sup>21</sup>E. Miletics and G. Molnárka, "Taylor series method with numerical derivatives for initial value problems," *J. Comput. Methods Sci. Eng.* **4**(1–2), 105–114 (2004), available at <https://dl.acm.org/doi/10.5555/1411367.1411380>.
- <sup>22</sup>E. Miletics and G. Molnárka, "Implicit extension of Taylor series method with numerical derivatives for initial value problems," *Comput. Math. Appl.* **50**(7), 1167–1177 (2005).
- <sup>23</sup>D. Ornstein, "Ergodic theory, randomness, and 'chaos,'" *Science* **243**(4888), 182–187 (1989).
- <sup>24</sup>N. H. Packard, J. P. Crutchfield, J. D. Farmer, and R. S. Shaw, "Geometry from a time series," *Phys. Rev. Lett.* **45**, 712 (1980).
- <sup>25</sup>M. Palus and M. Vejmelka, "Directionality of coupling from bivariate time series: How to avoid false causalities and missed connections," *Phys. Rev. E* **75**, 056211 (2007).
- <sup>26</sup>M. Planck, "Über irreversible strahlungsvorgänge," *Ann. Phys.* **306**(1), 69–122 (1900).
- <sup>27</sup>H. Poincaré, *Œuvres VII, 262–490 (Theorem 1 Section 8), Mécanique Céleste et Astronomie* (Gauthier-Villars, Paris, 1890).
- <sup>28</sup>H. Poincaré, "Sur le problème des trois corps et les équations de la dynamique," *Acta Math.* **13**, 1–270 (1890), available at <https://projecteuclid.org/journals/acta-mathematica/volume-13/issue-1-2>.
- <sup>29</sup>W. Press, B. Flannery, S. Teukolsky, and W. Vetterling, *Numerical Recipes in C* (Cambridge University Press, New York, 1990).
- <sup>30</sup>Y. Ruan, R. V. Donner, S. Guan, and Y. Zou, "Ordinal partition transition network based complexity measures for inferring coupling direction and delay from time series," *Chaos* **29**(4), 043111 (2019).
- <sup>31</sup>J. Runge, V. Petoukhov, J. F. Donges, J. Hlinka, N. Jajcay, M. Vejmelka, D. Hartman, N. Marwan, M. Paluš, and J. Kurths, "Identifying causal gateways and mediators in complex spatio-temporal systems," *Nat. Commun.* **6**, 8502 (2015).
- <sup>32</sup>T. Sauer, J. A. Yorke, and M. Casdagli, "Embedology," *J. Stat. Phys.* **65**, 579 (1991).
- <sup>33</sup>T. Schreiber, "Measuring information transfer," *Phys. Rev. Lett.* **85**, 461–464 (2000).
- <sup>34</sup>D. A. Smirnov, "Quantification of causal couplings via dynamical effects: A unifying perspective," *Phys. Rev. E* **90**, 062921 (2014).
- <sup>35</sup>G. Sugihara, R. May, H. Ye, C.-H. Hsieh, E. Deyle, M. Fogarty, and S. Munch, "Detecting causality in complex ecosystems," *Science* **338**(6106), 496–500 (2012).
- <sup>36</sup>F. Takens, "Detecting strange attractors in turbulence," in *Dynamical Systems and Turbulence, Warwick 1980*, Lecture Notes in Mathematics Vol. 898, edited by D. A. Rand and L.-S. Young (Springer, Berlin, 1981), pp. 366–381.
- <sup>37</sup>N. Wiener, *Modern Mathematics for Engineers, The Theory of Prediction* (McGraw Hill, New York, 1956), pp. 165–190.
- <sup>38</sup>Y. Zou, R. V. Donner, N. Marwan, J. F. Donges, and J. Kurths, "Complex network approaches to nonlinear time series analysis," *Phys. Rep.* **787**, 1–97 (2019).